ORIGINAL ARTICLE

Platelet Activation and Aggregation Promote Lung Inflammation and Influenza Virus Pathogenesis

Vuong Ba Lê[1]*, Jochen G. Schneider[2,3]*, Yvonne Boergeling[4], Fatma Berri[1], Mariette Ducatez[5,6], Jean-Luc Guerin[5,6], Iris Adrian[3], Elisabeth Errazuriz-Cerda[7], Sonia Frasquilho[8], Laurent Antunes[8], Bruno Lina[1], Jean-Claude Bordet[9], Martine Jandrot-Perrus[10], Stephan Ludwig[4], and Béatrice Riteau[1,11]

[1]EA4610, Lyon, France; [2]Luxembourg Centre for Systems Biomedicine, Esch-Sur-Alzette, Luxembourg; [3]Saarland University Medical Center, Homburg/Saar, Germany; [4]Institute Molecular Virology, ZMBE, Münster, Germany; [5]UMR 1225, IHAP, INRA, Toulouse, France; [6]INP, ENVT, Toulouse France; [7]Centre Commun d'Imagerie Quantitative Lyon Est, SFR Santé Lyon-Est, University of Lyon, Lyon, France; [8]Integrated BioBank of Luxembourg, For Next Generation Healthcare, Luxembourg, Luxembourg; [9]Unité d'Hémostase Clinique, Lyon, France; [10]INSERM UMR_S1148, Paris Diderot, CHU Xavier Bichat, Paris, France; and [11]UMR1062 INSERM INRA, Faculté de Medécine La Timone, Marseille, France

Abstract

Rationale: The hallmark of severe influenza virus infection is excessive inflammation of the lungs. Platelets are activated during influenza, but their role in influenza virus pathogenesis and inflammatory responses is unknown.

Objectives: To determine the role of platelets during influenza A virus infections and propose new therapeutics against influenza.

Methods: We used targeted gene deletion approaches and pharmacologic interventions to investigate the role of platelets during influenza virus infection in mice.

Measurements and Main Results: Lungs of infected mice were massively infiltrated by aggregates of activated platelets. Platelet activation promoted influenza A virus pathogenesis. Activating protease-activated receptor 4, a platelet receptor for thrombin that is crucial for platelet activation, exacerbated influenza-induced acute lung injury and death. In contrast, deficiency in the major platelet receptor glycoprotein IIIa protected mice from death caused by influenza viruses, and treating the mice with a specific glycoprotein IIb/IIIa antagonist, eptifibatide, had the same effect. Interestingly, mice treated with other antiplatelet compounds (antagonists of protease-activated receptor 4, MRS 2179, and clopidogrel) were also protected from severe lung injury and lethal infections induced by several influenza strains.

Conclusions: The intricate relationship between hemostasis and inflammation has major consequences in influenza virus pathogenesis, and antiplatelet drugs might be explored to develop new antiinflammatory treatment against influenza virus infections.

Keywords: lung injury; novel drugs; flu pathogenesis; pneumonia; platelets

At a Glance Commentary

Scientific Knowledge on the Subject: During severe influenza, dysregulation of cytokine production contributes to lung damage. Platelets are activated during influenza, but their role in influenza virus pathogenesis and inflammatory responses is unknown.

What This Study Adds to the Field: This study shows that during severe influenza A virus infection in mice, platelet activation worsens the severity of lung injury. Antiplatelet drugs might be explored to develop new antiinflammatory treatment against influenza virus infections.

(Received in original form June 5, 2014; accepted in final form February 4, 2015)

*These authors contributed equally to this work as co–first authors.

Supported by ANR (ANR-13-BSV3-0011, HemoFlu [B.R. and M.J.-P.]), DFG (SCH682/3-1 [J.G.S.]), EU CIG303682, and FNR CORE Itgb3VascIn.

Author Contributions: V.B.L., J.G.S., J.-C.B., M.J.-P., S.L., and B.R. designed the experiments. V.B.L., Y.B., F.B., M.D., J.-L.G., I.A., E.E.-C., S.F., and L.A. performed the experiments. F.B., J.G.S., S.L., and B.L. critically read the manuscript. V.B.L., M.J.-P., and B.R. wrote the manuscript.

Correspondence and requests for reprints should be addressed to Béatrice Riteau, Ph.D., UMR 1062, Faculté de Medécine Secteur Timone, 27 Bd Jean Moulin, Marseille, France. E-mail: beatrice.riteau@laposte.net

Am J Respir Crit Care Med Vol 191, Iss 7, pp 804–819, Apr 1, 2015

Originally Published in Press as DOI: 10.1164/rccm.201406-1031OC on February 9, 2015
Internet address: www.atsjournals.org

Influenza is one of the most common infectious diseases in humans, occurring as sporadic pandemic and seasonal epidemic outbreaks leading to significant numbers of fatalities. Influenza pathogenesis is a complex process involving both viral determinants and the immune system (1–3). During severe influenza, dysregulation of cytokine production contributes to lung damage, possibly leading to organ failure and death (4–6). The endothelium, which lines the interior surface of the blood vessels, is thought to orchestrate the crescendo in cytokine accumulation, although the mechanism involved is not fully understood (7).

On endothelial injury, platelets are recruited by inflamed endothelial cells, where they adhere and are activated (8). Simultaneously, the family of protease-activated receptors (PARs) mediates platelet activation by thrombin. PAR4 is strictly required for platelet activation in mice, because mouse platelets do not express PAR1. In contrast, both PAR1 and PAR4 are important for platelet activation in humans. These events lead to a conformational change in the platelet glycoprotein IIb/IIIa (GPIIb/IIIa) receptor for fibrinogen that bridges platelets, leading to their aggregation and a reinforcement of their activation. Importantly, platelet activation is strongly associated with enhanced inflammatory responses. Activated platelets release potent inflammatory molecules and play a key role in leukocyte recruitment (9). Platelet activation is finely tuned, but its dysfunction is pathogenic and contributes to inflammatory disorders (10, 11). Thus, uncontrolled platelet activation could contribute to the pathogenesis of influenza A virus (IAV) infections by fueling a harmful inflammatory response in the respiratory tract. However, the role of platelets in the context of IAV infection has never been investigated. In the present study, using pharmacologic and gene deletion approaches, we investigated the role of platelets in IAV pathogenesis *in vivo*. We found that during severe IAV infection in mice, platelet activation worsens the severity of lung injury.

Methods

Reagents

A549 cells and MDCK cells were purchased from ATCC (Molsheim Cedex, France). IAV A/PR/8/34 (H1N1), A/HK/1/68 (H3N2), and A/NL/602/2009 (H1N1) viruses (ATCC) were gifts from G. F. Rimmelzwaan (Erasmus, the Netherlands). The highly pathogenic avian A/FPV/Bratislava/79 (H7N7) strain was from the Institute of Molecular Virology (Münster, Germany). The following reagents were used: 4′,6-diamidino-2-phenylindole (DAPI) (Life Technologies, Paris, France); Alexa Fluor secondary antibodies (Life Technologies); eptifibatide (Integrilin, GlaxoSmithKline, Marly-le-Roi, France); Clopidogrel (Santa Cruz Biotechnology, Heidelberg, Germany); MRS 2179 (Tocris Bioscience, Bristol, UK); PAR4 antagonist pepducin p4pal-10 (Polypeptide Laboratories, Strasbourg, France); PAR4 agonist peptide (AYPGKF-NH2 [PAR4-AP]; Bachem, Weil-am-Rhein, Germany); PAR4 control peptide (YAPGKF-NH2 [Control-P]; Bachem); monoclonal antineutrophil Ly6G (Cedarlane; Tebu-bio, Le Perray en Yvelines, France); polyclonal antiplatelet CD41 (Bioss, Woburn, MA); monoclonal antiviral antihemagglutinin (HA) (Santa Cruz Biotechnology); monoclonal anti-IAV nucleoprotein (NP) (gift from G. F. Rimmelzwaan); monoclonal anti–P-selectin fluorescein isothiocyanate–conjugated (Emfret, Eibelstadt, Germany); monoclonal anti-CD41/61 phycoerythrin-conjugated (Emfret); Vectastain ABC kit (Vector Laboratories, Burlingame, CA); 3,3′-diaminobenzidine peroxidase substrate (Vector Laboratories); ketamine/xylazine anesthesia (Virbac; Bayer HealthCare, Carros, France); May-Grünwald and Giemsa solutions (Merck, Darmstadt, Germany); hematoxylin and eosin (H&E) solutions (Diapath, Martinengo, Italy); and ELISA kits for mouse IL-6, IL-1β, macrophage inflammatory protein (MIP)-2 (PromoCell GmbH, Heidelberg, Germany), IFN-α, IFN-γ, regulated on activation normal T-cell expressed and secreted (R&D Systems, Lille, France), serotonin (BlueGene, Shanghai, China), thromboxane B_2 (TXB_2; Elabscience, Wuhan, China), and soluble P-selectin (sP-selectin; Qayee-Bio, Shanghai, China). Total protein was evaluated by using the Coomassie Bradford Protein assay kit (Thermo Scientific, Franklin, MA).

Mice

Experiments were performed in accordance with the Guide for the Care and Use of Laboratory Animals of the Direction des Services Vétérinaires, the French regulations to which our animal care and protocol adhered. The license authority was issued by the Direction des Services Vétérinaires and Lyon University (accreditation 78–114). Protocols were approved by the Committee on Ethics of Animal Experiments of Lyon University (Permit BH2008–13).

Female, 7-week-old BALB/c mice were used for H7N7 virus infections. Otherwise, 6-week-old C57BL/6 female mice (Charles River Laboratories, Arbresle, France) and $GPIIIa^{-/-}$ mice or wild-type (WT) littermates on a C57BL/6 background were used in this study. For the latter, heterozygous mice were crossed, and WT and knock-out offspring (males and females) were used. Polymerase chain reaction of tail-tip genomic DNA was performed (12) to determine the absence or presence of the GPIIIa gene. Infection experiments were performed as previously described (13). Mice were anesthetized with ketamine/xylazine (42.5/5 mg/kg) and inoculated intranasally with IAV, in a volume of 20 μl. Eptifibatide was injected intraperitoneally (500 μg/kg or 10 μg/200 μl per mouse of ∼20 g body weight) every 3 days until the end of the experiment. MRS 2179 was dissolved in saline buffer and administered once intravenously (50 mg/kg) on Day 0. Clopidogrel dissolved in saline buffer was injected intraperitoneally (30 mg/kg) every day until the end of the experiment.

For PAR4 stimulation experiments, mice were anesthetized every day for 3 days. On the first day, the anesthetized mice were infected intranasally in the presence or absence of PAR4-AP or Control-P (100 μg per mouse, in a volume of 20 μl). Intranasal peptide treatments were also repeated on Days 2 and 3 after infection. For PAR4 antagonist treatment, pepducin p4pal-10 was given intraperitoneally (0.5 mg/kg) 2 days postinfection, and treatments were repeated on the next 2 days.

On inoculation, the survival rates were followed. Alternatively, mice were killed at prefixed time points to perform bronchoalveolar lavage (BAL) or harvest lungs. ELISA was performed according to the manufacturers' instructions. Virus titers were assessed as previously described (14). Lungs were also harvested for histology and immunohistochemistry as previously described (15).

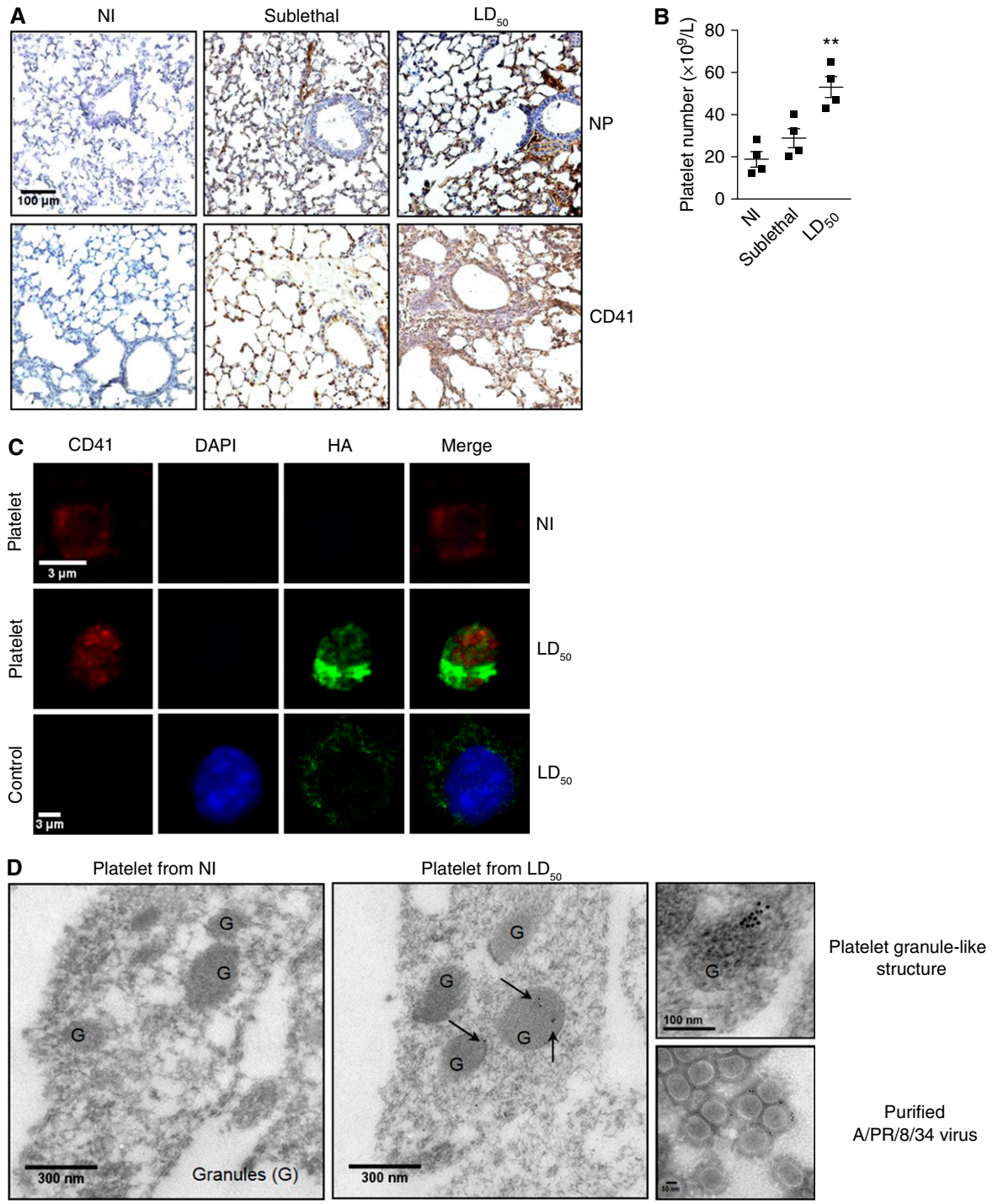

Figure 1. On influenza A virus (IAV) infection, platelets infiltrate the lungs, and IAV particles are observed in platelets. (*A*) Immunohistochemistry analysis of lungs from uninfected (NI) or infected mice inoculated with A/PR/8/34 virus, at a sublethal dose (75 pfu per mouse) or 50% lethal dose (LD_{50}) (250 pfu per mouse; Day 6 postinfection). Antibodies against the IAV nucleoprotein (NP) and CD41 were used to detect virus-infected cells and platelets, respectively. The results are representative of three mice per group. (*B*) Platelet numbers in bronchoalveolar lavage (BAL) were assessed using a Vet ABCTM Hematology Analyzer on Day 6 postinoculation of mock- or IAV-infected mice. Data are presented as the means ± SEM of four mice per group, $^{**}P < 0.01$ for LD_{50} versus NI. (*C*) Immunofluorescence staining of viral particles in platelets from BAL was performed with antiinfluenza antihemagglutinin (HA) antibody. Platelets were detected with anti-CD41 antibody, and nuclei were counterstained with 4′,6-diamidino-2-phenylindole (DAPI). The merged images are shown on the *right*. CD41-negative cells from BAL were used as a negative control. (*D*) Immunogold labeling of ultrathin cryosections of lungs of NI or A/PR/8/34 virus–infected mice (LD_{50}; 250 pfu per mouse; Day 6 postinfection) was performed using a specific anti-HA antibody. *Arrows* indicate viral particles. Staining of a platelet granule-like structure is shown on the *upper right*. As a control for HA staining, electron microscopic immunogold labeling was performed on purified A/PR/8/34 viruses using the anti-HA antibody (*lower right*).

Evaluation of Hemorrhagic Foci by Histopathologic Analysis

Lungs from mice inoculated with A/PR/8/34 virus (250 PFU per mouse) with or without eptifibatide treatment were fixed in 10% neutral buffered formalin and embedded in paraffin. Then, 4- to 6-μm sections were cut and stained with H&E to evaluate histopathologic changes. Staining was performed by incubation of the lung sections with Harris hematoxylin for 6 minutes, running tap water for 1 minute, eosin Y for 10 minutes, 70% ethanol for 1 minute, 95% ethanol for 1 minute, 100% ethanol for 1 minute, and two rinses in 100% xylene for 1 minute. Histology and injury scoring were performed by a masked investigator who analyzed the samples and determined the levels of injury according to a semiquantitative scoring system (counting inflammatory infiltration, vascular congestion, hemorrhage, fibrin deposits, and epithelial cell apoptosis).

Microscopy

For ultrastructural analysis, lung tissues were cut into 1-mm^3 pieces, fixed in 2% glutaraldehyde at 4°C, washed in 0.2 M cacodylate-HCl buffer containing 0.4 M saccharose and post-fixed in 0.3 M cacodylate-HCl buffer containing 2% osmium tetroxide for 1 hour. After dehydration in a graded alcohol series, tissue samples were impregnated with a 75% Epon A/25% Epon B/1.7% DMP30 mixture. Tissue embedding entailed polymerization at 60°C for 72 hours. Then, 70-nm sections were cut using an ultramicrotome (Leica Microsystems, Mannheim, Germany), mounted on 200-mesh copper grids coated with 1:1,000 polylysine, stabilized for 24 hours and contrasted with uranyl acetate/citrate. Sections were examined using a transmission electron microscope (JEOL 1400; JEOL, Tokyo, Japan) at 80 kV equipped with an Orius SC600 camera (Gatan, France). Immunogold staining was performed using the anti-HA antibody followed by 10-nm gold-conjugated secondary antibody, as previously described (16). As a control of HA labeling, we used IAV particles that we recently purified (17).

Fluorescence Microscopy Experiments

Cells from the BAL were centrifuged at 1,800 rpm for 5 minutes at room temperature and

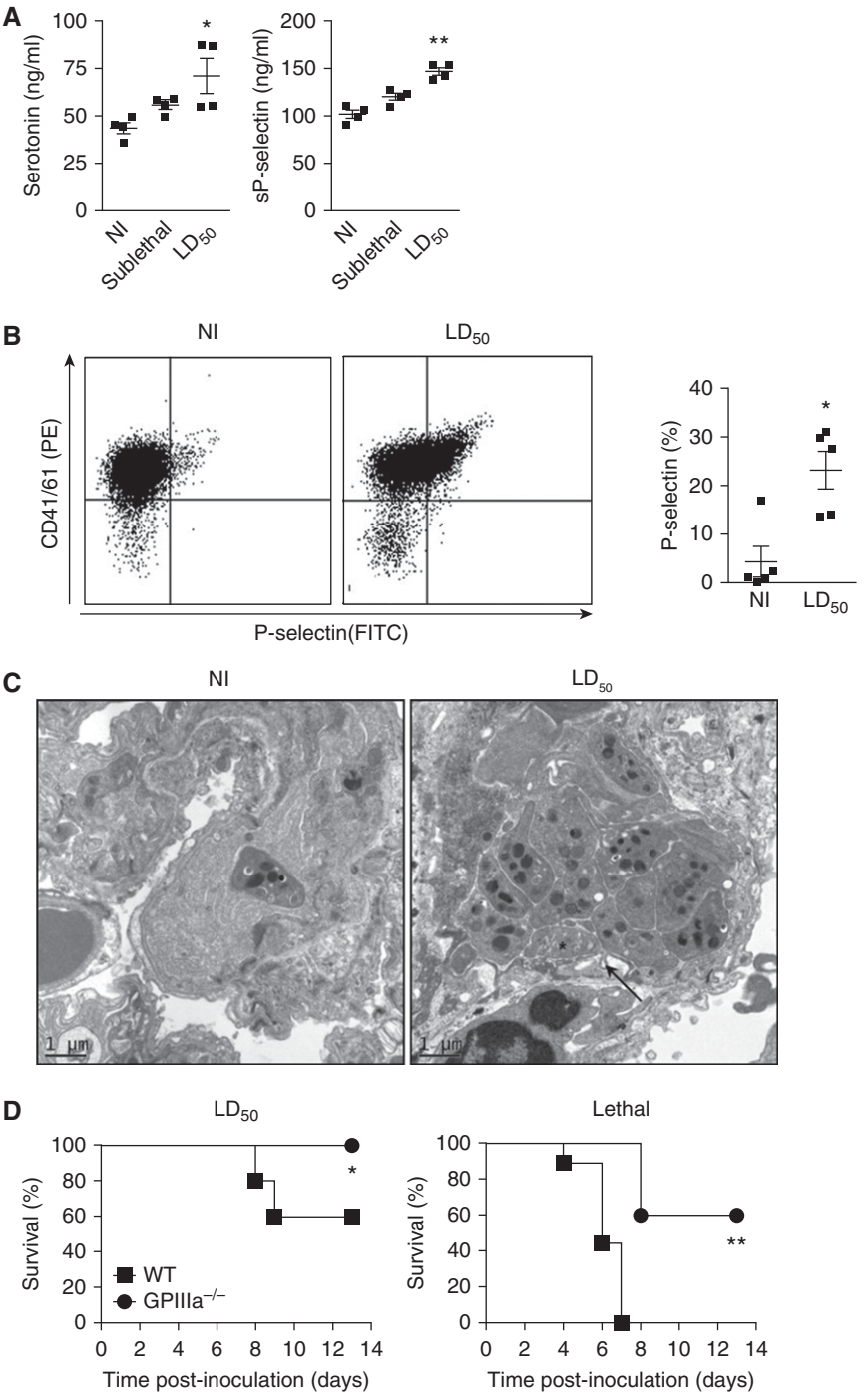

Figure 2. On influenza A virus infection, platelets are stimulated and contribute to influenza pathogenesis. (*A*) Serotonin and soluble P-selectin (sP-selectin) were measured by ELISA in the bronchoalveolar lavage and plasma of mock- (NI) or A/PR/8/34 virus–infected mice, respectively, on Day 6 postinoculation (75 pfu per mouse; sublethal dose or 250 pfu per mouse; 50% lethal dose [LD_{50}]). Data represent the means ± SEM of four mice per group, $^*P < 0.05$ for LD_{50} versus NI; $^{**}P < 0.01$ for LD_{50} versus NI. (*B*) Blood samples from uninfected (NI) or infected mice were double-stained with anti–P-selectin and anti-CD41 antibody as a platelet identifier. The mean percentage ± SEM of activated platelets (CD41 and P-selectin–positive) from five mice per group is shown in the *right*, $^*P < 0.05$ for LD_{50} versus NI. (*C*) Ultrastructure analysis of platelets in the lungs of uninfected and infected mice (A/PR/8/34; 250 pfu per mouse; LD_{50}). Note the aggregation of platelets in the lungs of infected mice along with their morphologic changes (*arrow*) and the absence

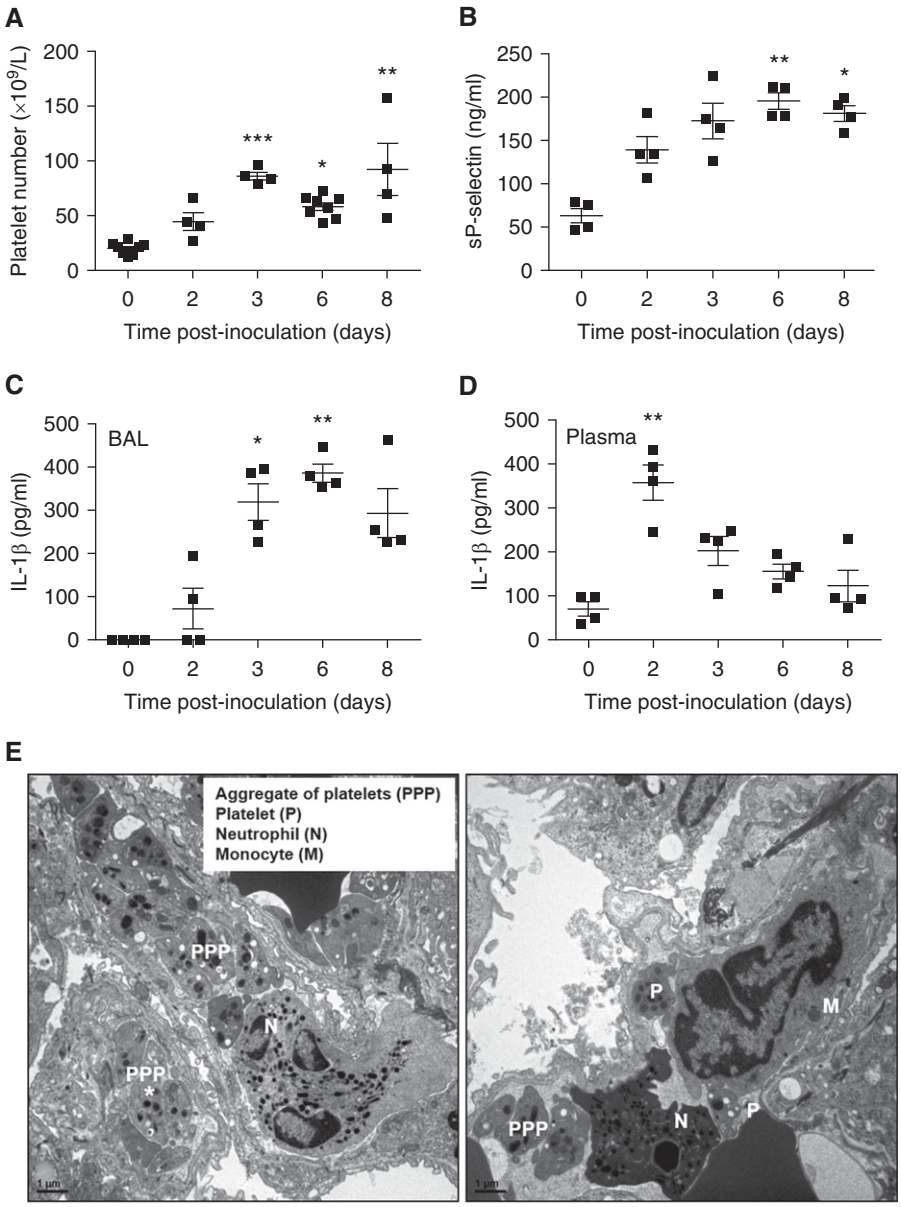

Figure 3. Platelet activation and inflammation. (*A*) Platelet numbers in bronchoalveolar lavage (BAL) of A/PR/8/34 virus–infected mice (250 pfu per mouse; 50% lethal dose [LD_{50}]) were assessed using a Vet ABCTM Hematology Analyzer, at the indicated time postinoculation. The results are represented as the means ± SEM of four mice per group. On Days 0 and 6, additional results from Figure 1B are included. (*B–D*) Soluble P-selectin (sP-selectin) in the plasma (*B*), IL-1β in the BAL (*C*), and IL-1β in the plasma (*D*) of infected mice (A/PR/8/34; 250 pfu per mouse; LD_{50}) were determined by ELISA at the indicated times. The results from *B–D* represent the means ± SEM of four mice per group. From *A–D*: $^{*}P < 0.05$, $^{**}P < 0.01$, $^{***}P < 0.001$ for the indicated time versus 0. (*E*) Ultrastructural analysis of platelets associated with leukocytes in the lungs of infected mice (A/PR/8/34; 250 pfu per mouse; LD_{50}). The *asterisk* shows platelet aggregates that are not adherent to leukocytes.

suspended in phosphate-buffered saline at a concentration of 5×10^5 per milliliter. Then, 100 μl of the solution was used to centrifuge the cells onto coverslips (1,000 rpm for 5 min) using a Shandon Cytospin 4 centrifuge (Thermo Scientific, Illkirch, France). The slides were then dipped in a box containing methanol and kept at −20°C for fixation and permeabilization. After 10 minutes, cells were extensively washed with phosphate-buffered saline to remove the fixative. Cells were then incubated with primary antibodies to CD41 and viral HA for 1 hour at room temperature. Revelation was performed using Alexa Fluor (Life Technologies) secondary antibodies for 1 hour at room temperature. Cells were also counterstained with DAPI for 15 minutes at room temperature. Images were analyzed using a Leica TCS SP5 confocal system (Leica Microsystems).

Evaluation of Platelet and Leukocyte Numbers

Platelets were counted using the Vet ABC Hematology Analyzer (SCIL Animal Care Company Sarl, Altorf, France) using the mouse smart card 7030. The automated cell counter differentiates mouse platelets based on their size in multiple sample fluids. Leukocytes and neutrophils in the BAL were visualized by May-Grünwald-Giemsa–stained cytospin preparations, as previously performed (13).

Flow Cytometry of Blood Platelets

Blood was collected in ACD buffer by cardiac puncture. CD41-positive cells and platelet activation in whole blood were evaluated using fluorescein isothiocyanate–conjugated P-selectin and phycoerythrin-conjugated CD41/CD61 antibodies, as previously described (18, 19).

Statistical Analysis

The Kaplan-Meier test was used for survival rates. The Mann-Whitney test was used for two-group comparisons of mean percentages in the flow cytometry experiments, lung virus titers, ELISA, and total protein quantifications. One-way analysis of variance for nonparametric measures (Kruskal-Wallis) was used for multiple-group comparisons in dose–responses or kinetics experiments. Dunn multiple comparison test was used as a *post hoc* test using uninfected mice as a control animal. *P* less than 0.05 was considered statistically significant.

Figure 2. (Continued). of granules in some of them, which reflects their degranulation (*asterisk*). Sections show platelet aggregates with an interstitial localization. (*D*) Survival of platelet glycoprotein (GP) $IIIa^{-/-}$ mice and wild-type (WT) littermates after infection with A/PR/8/34 virus at a LD_{50} (250 pfu per mouse; n = 9–10 mice per group) or lethal dose (350 pfu per mouse; n = 6 mice per group); $^{*}P < 0.05$ and $^{**}P < 0.01$, respectively. FITC = fluorescein isothiocyanate; PE = phycoerythrin.

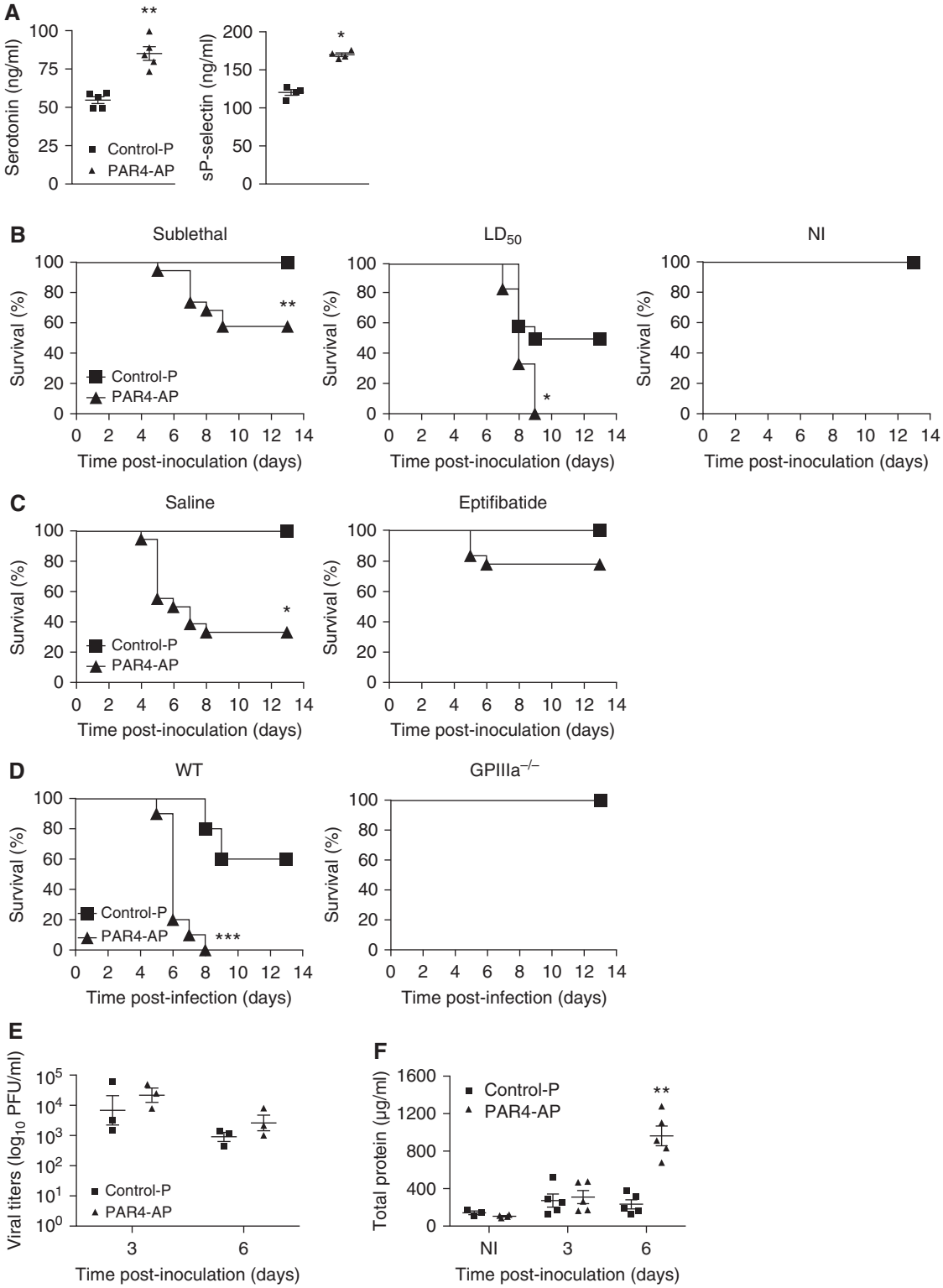

Figure 4. Effects of protease-activated receptor (PAR) 4 activation on influenza A virus (IAV) pathogenicity, virus replication, and inflammation. (*A*) Serotonin and soluble P-selectin (sP-selectin) were measured by ELISA in the bronchoalveolar lavage (BAL) and plasma, respectively, of infected mice (A/PR/8/34; 75 pfu per mouse; sublethal dose) after treatment with PAR4 agonist peptide (PAR4-AP) or control peptide (Control-P) on Day 6 postinoculation. Data are shown as means ± SEM (n = 4–5). $^{*}P < 0.05$; $^{**}P < 0.01$. (*B*) Time course of IAV-induced death in mice in response to PAR4 stimulation. Mice were mock infected (NI) or inoculated with A/PR/8/34 virus (75 pfu per mouse, sublethal dose, n=18–19 mice per group; or 250 pfu per mouse, 50% lethal dose [LD_{50}], n = 6–12 mice per group) and treated with either Control-P or PAR4-AP. $^{*}P < 0.05$; $^{**}P < 0.01$. (*C*) Time course of

Results

Platelet Recruitment to the Lungs on IAV Infection

Platelet recruitment to the lungs was first examined after infection of mice with a sublethal or a 50% lethal dose (LD_{50}) of IAV A/PR/8/34. Immunohistochemistry of the lungs, using monoclonal antibodies for IAV NP and CD41, was used to detect virus-infected cells and platelets, respectively (Figure 1A). At both doses, many IAV-infected cells and marked platelet infiltrates were detected in the lungs of infected mice compared with uninfected mice. To confirm these results, platelet counts in the BAL of infected versus uninfected mice (sublethal dose or LD_{50}) were assessed using a blood cell counter (Figure 1B). In the BAL of infected mice, the platelet levels increased in a dose-dependent manner and were significantly higher than in those of uninfected mice, reaching 50×10^9 cells per liter on Day 6 postinoculation (LD_{50}). Differences were not significant on infection with IAV at the sublethal dose.

Viral Proteins Are Present within Platelets

The presence of viral proteins was next determined in platelets from the BAL of infected mice. Platelets were identified by immunofluorescence as CD41-positive, DAPI-negative elements, and IAV particles were detected using the viral HA antibody. In contrast to uninfected mice, on infection (LD_{50}), CD41-positive DAPI-negative platelets stained positively for viral HA, demonstrating that platelets engulfed IAV particles, fragments of IAV, or viral proteins *in vivo* (Figure 1C). CD41-negative/DAPI-positive cells were used as controls for antibody specificity. To confirm these results, immunogold labeling of ultrathin cryosections of lungs from uninfected or infected mice was performed using a specific anti-HA antibody. Examination of platelets clearly showed a positive and specific staining of viral HA proteins, which were located predominantly within platelet granule-like structures (Figure 1D, *middle* and *upper right*). The sparse staining could have been caused by the procedure. Indeed, as a control, we used immunogold labeling of HA on highly purified A/PR/8/34 virus particles (17). Although virions of IAV contain approximatively 500 molecules of HA per virion, few gold particles were observed (Figure 1D, *lower right*).

Platelet Activation and Aggregation

On activation, platelets become immobilized, secrete their granule content, and aggregate. Serotonin is released from platelet-dense granules, and P-selectin is rapidly translocated from the alpha granules to the plasma membrane and shed. Thus, we next analyzed these responses in the lungs of infected mice (sublethal or LD_{50}). Serotonin and sP-selectin were measured in BAL and plasma, respectively, by ELISA (Figure 2A). Serotonin and sP-selectin were significantly higher in the fluid of infected mice compared with uninfected mice. Significant differences were only observed on infection with IAV at LD_{50}. Furthermore, exposure of P-selectin on the surface of platelets isolated from IAV-infected mice was increased compared with uninfected mice (Figure 2B, *left*). The average percentage of P-selectin–positive platelets reached 23% on infection, versus 5% in uninfected mice (Figure 2B, *right*). Moreover, transmission electron microscopy showed that platelets in the lungs of influenza virus–infected mice were tightly packed, forming large extravascular aggregates with signs of shape change and some platelets were devoid of granules (Figure 2C). In contrast, in the lungs of uninfected mice, only a few isolated platelets were detected.

Platelets Contribute to Influenza Pathogenesis

Platelet GPIIIa$^{+/-}$ mice were intercrossed to generate WT and platelet GPIIIa$^{-/-}$ mice, which were then infected with IAV A/PR/8/34, and the survival rates were monitored. As shown in Figure 2D, compared with WT mice, GPIIIa$^{-/-}$ mice were significantly more resistant to IAV-induced death.

Time Course of Platelet Activation, IL-1β Release, and Platelet Binding to Leukocytes

Platelets were counted in the BAL of infected mice (LD_{50}) at various times postinoculation. On infection, platelet counts increased in a time-dependent manner (Figure 3A), peaked on Day 3, and stayed elevated until Day 8. Plasmatic sP-selectin significantly increased during the course of infection and plateaued on Days 3–8 (Figure 3B). Increased IL-1β was also detected in the BAL and blood of infected mice but with different lags (Figures 3C and 3D). IL-1β released in the BAL paralleled platelet activation, whereas IL-1β peaked in the blood on Day 2 postinoculation and then rapidly decreased. Ultrastructural analysis of the lungs of A/PR/8/34-infected mice showed that platelet-leukocyte complexes formed *in vivo*. Neutrophils and monocytes were associated with platelet aggregates, although not all platelets adhered to leukocytes (Figure 3E).

PAR4 Promotes Pathogenesis of IAV Infection in a Platelet-Dependent Pathway

Mice were inoculated with a sublethal dose of IAV A/PR/8/34 and stimulated with 100 μg per mouse of PAR4-AP or Control-P. As expected, the content of serotonin and sP-selectin was increased in the BAL of infected mice treated with PAR4-AP compared with Control-P, indicating an increased level of platelet activation (Figure 4A). More interestingly, on infection, mice treated with PAR4-AP displayed significantly higher mortality rates compared with mice treated with Control-P (Figure 4B). In contrast, treatment with PAR4-AP did not affect the survival of uninfected mice. The effect

Figure 4. (Continued). IAV-induced death in mice (A/PR/8/34 virus) in response to PAR4 stimulation and after treatment or no treatment with eptifibatide (n = 6–18 mice per group). $^*P < 0.05$ for PAR4-AP versus Control-P. A significant difference ($P < 0.01$) was also found between groups treated with PAR-AP ± eptifibatide (not shown). (*D*) Time course of IAV-induced death in wild-type (WT) (n = 10 mice per group) and glycoprotein (GP) IIIa$^{-/-}$ mice (n = 7–9 mice per group) in response to PAR4 stimulation (A/PR/8/34 virus). The same mice were used in Figure 2D (250 pfu per mouse; dose LD_{50}). $^{***}P < 0.001$ for PAR4-AP versus Control-P in WT mice. (*E*) Lung virus titers after infection of mice with A/PR/8/34 virus (sublethal dose) stimulated or not with PAR4-AP. (*F*) Total protein quantification in BAL of infected mice in response to PAR4 stimulation. For *E* and *F*, the results represent the means ± SEM (n = 3–5). $^{**}P < 0.01$ for PAR4-AP versus Control-P.

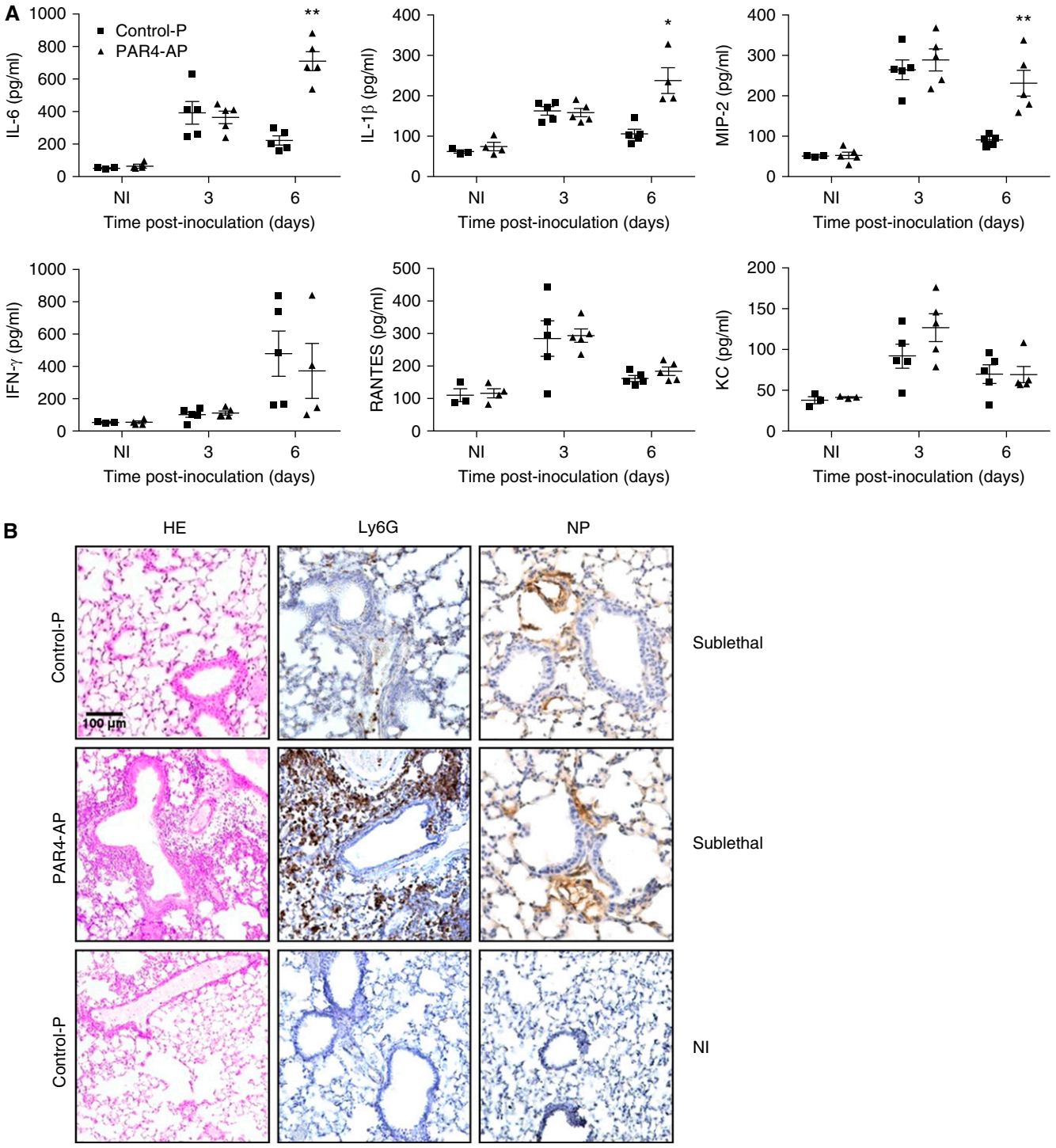

Figure 5. Protease-activated receptor (PAR) 4 agonist peptide (PAR4-AP) increases lung inflammation on A/PR/8/34 virus infection. (*A*) Cytokines in the bronchoalveolar lavage of infected mice (75 pfu per mouse; sublethal dose), treated with PAR4-AP or control peptide (Control-P), were measured by ELISA 3 and 6 days after inoculation. Uninfected mice (NI) were used as control animals. The results represent the means ± SEM (n = 3–5). $^{*}P < 0.05$, $^{**}P < 0.01$ for PAR4-AP versus Control-P. (*B*) Histopathologic analysis of lungs from uninfected mice or mice infected with a sublethal dose (75 pfu per mouse) of A/PR/8/34 virus after treatment with PAR4-AP or Control-P, on Day 6 postinfection. Thin sections of lungs were stained with hematoxylin and eosin (HE). Note the marked infiltration of cells in the lungs of infected mice stimulated with PAR4-AP. Immunohistochemistry used antibodies against Ly6G. Viral nucleoprotein (NP) was used to detect neutrophils and virus-infected cells. Data are representative of three mice per group. KC = keratinocyte chemoattractant; MIP = macrophage inflammatory protein; RANTES = regulated on activation normal T-cell expressed and secreted.

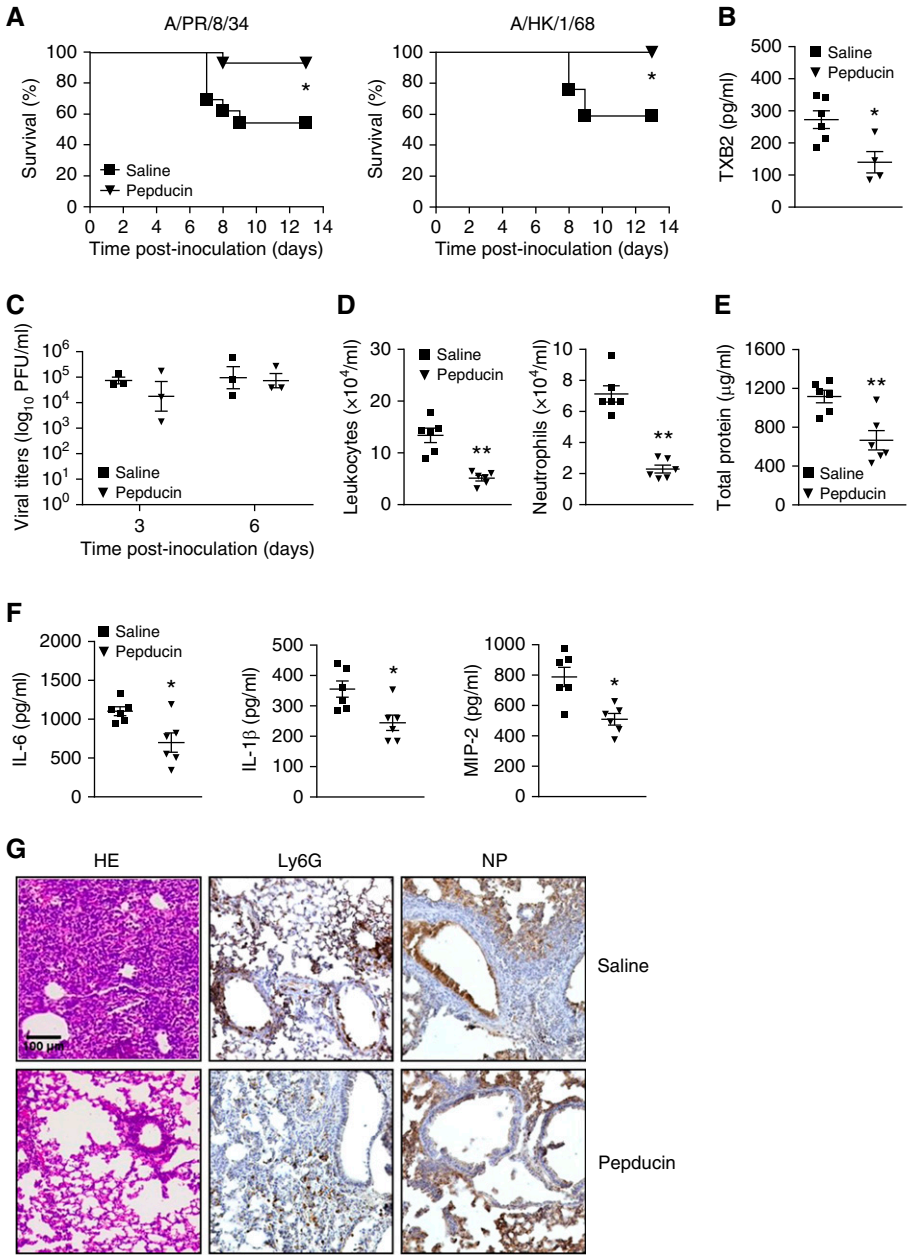

Figure 6. Protease-activated receptor (PAR) 4 antagonist protects mice against influenza A virus (IAV) infection and deleterious lung inflammation. (*A*) IAV-induced pathogenesis in mice treated or not with the PAR4 antagonist pepducin p4pal-10 (pepducin). Mice were inoculated with A/PR/8/34 virus (250 pfu per mouse; 50% lethal dose [LD_{50}]; n = 13 mice per group) or A/HK/1/68 (100 pfu per mouse; LD_{50}, n = 12 mice per group) and treated with pepducin or saline. Survival was then monitored for 2 weeks. *$P < 0.05$. (*B*) Thromboxane B_2 (TXB_2) was measured by ELISA in the bronchoalveolar lavage (BAL) of infected mice (A/PR/8/34; 250 pfu per mouse; LD_{50}) after treatment with pepducin or vehicle, on Day 6 postinoculation. Data represent the means ± SEM of four to six mice per group. (*C*) Lung virus titers after infection of mice with A/PR/8/34 virus (250 pfu per mouse; LD_{50}) treated with pepducin or vehicle. The results represent the means ± SEM from three individual animals per group. (*D*) Relative leukocyte and neutrophil numbers in BAL from mice treated with pepducin or vehicle, determined by May-Grünwald-Giemsa staining 6 days after inoculation. Data represent the means ± SEM from six individual mice per group. (*E* and *F*) Total proteins and levels of cytokines were determined by ELISA in the BAL of infected mice (A/PR/8/34; 250 pfu per mouse; LD_{50}) after treatment with pepducin or vehicle, on Day 6 postinoculation. The results represent the means ± SEM of six mice per group. (*G*) Histopathologic analysis of lungs from mice infected with A/PR/8/34 virus (250 pfu per mouse; LD_{50}) after treatment with pepducin or vehicle, on Day 6 postinfection. Lung sections were stained with hematoxylin and eosin (HE). Immunohistochemistry using antibodies against Ly6G or viral nucleoprotein (NP) was used to detect neutrophils and virus-infected cells. Data are representative of three mice per group. (*B–F*) *$P < 0.05$, **$P < 0.01$ for pepducin versus saline. MIP-2 = macrophage inflammatory protein-2.

was platelet dependent, because treatment of mice with eptifibatide, an antagonist of the GPIIbIIIa platelet receptor, abrogated the deleterious effect of PAR4-AP (Figure 4C), as did the platelet GPIIIa deficiency (Figure 4D). This indicated that PAR4-AP–induced platelet aggregation increased the severity of the IAV symptoms.

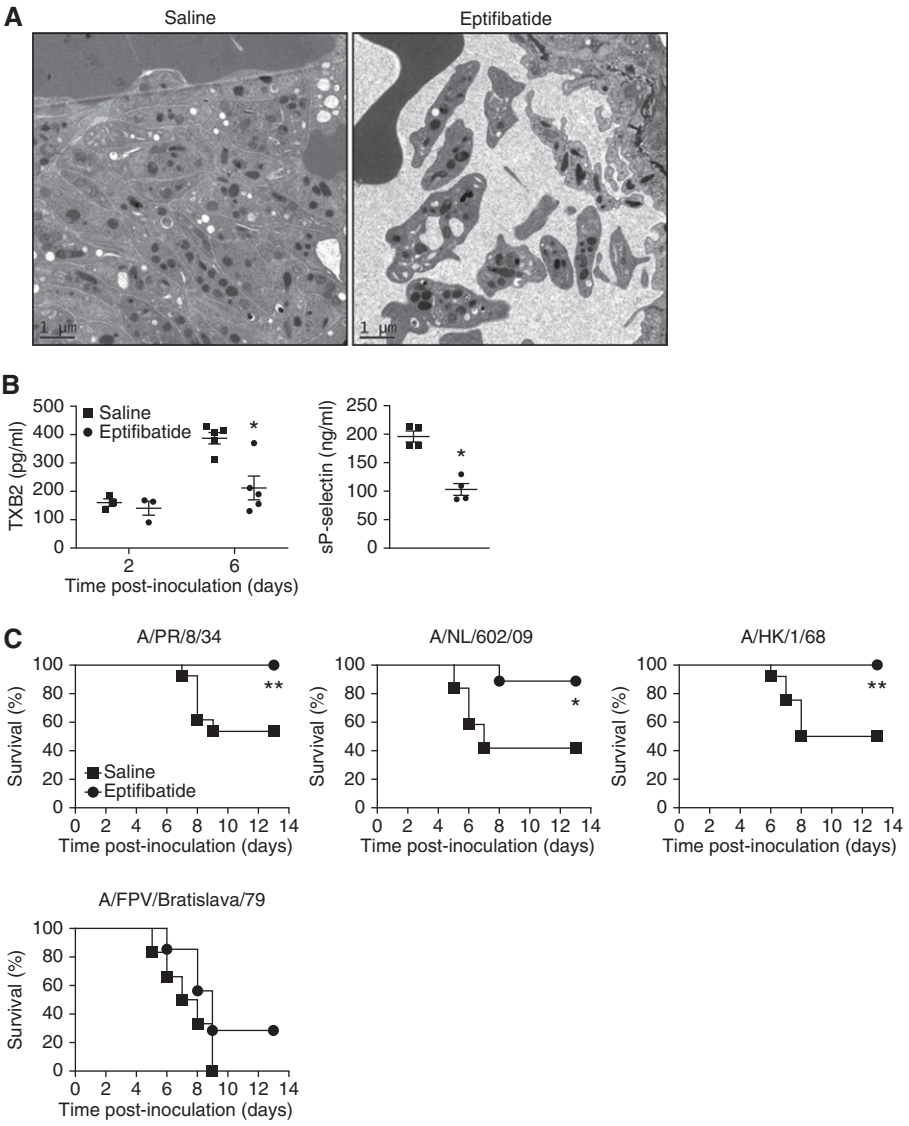

Figure 7. Eptifibatide protects mice against influenza A virus infection, independently of the strain. (*A*) Ultrastructural analysis of platelets in the lungs of infected mice (A/PR/8/34; 250 pfu per mouse; 50% lethal dose [LD_{50}]), treated or not with eptifibatide, was performed by transmission electron microscopy. Note the aggregation of platelets in the lungs of infected mice, and their disaggregation after treatment of mice with eptifibatide. Sections show platelet aggregates with an interstitial localization. (*B*) Thromboxane B_2 (TXB_2) was measured by ELISA in the bronchoalveolar lavage of infected mice (A/NL/602/09; 30,000 pfu per mouse; LD_{50}) after treatment with eptifibatide or vehicle. The results represent the means ± SEM of three to five mice per group. Soluble P-selectin (sP-selectin) was measured by ELISA in the plasma of A/PR/8/34 virus–infected mice (250 pfu per mouse; LD_{50}) that were treated or not with eptifibatide, on Day 6 postinoculation. Data represent the means ± SEM of four mice per group. $^{*}P < 0.05$ for pepducin versus saline. (*C*) Survival of mice treated with eptifibatide or vehicle after infection with influenza A virus A/PR/8/34 (n = 13 mice per group; 250 pfu per mouse), A/NL/602/09 (n = 9–12 mice per group; 30,000 pfu per mouse), or A/HK/1/68 (n = 12 mice per group; 100 pfu per mouse) at their respective LD_{50} values. A/FPV/Bratislava/79 was used at 5 pfu per mouse (n = 6–7 mice per group). $^{*}P < 0.05$, $^{**}P < 0.01$ for pepducin versus saline.

No significant differences in lung virus titer were observed 3 or 6 days postinoculation between mice treated with PAR4-AP and those treated with Control-P (Figure 4E). However, on Day 6, treatment with PAR4-AP significantly increased total proteins in the BAL (Figure 4F). The response levels of IL-6, IL-1β, and MIP-2 were also enhanced, whereas those of IFN-γ, regulated on activation normal T-cell expressed and secreted, and keratinocyte chemoattractant were unaffected (Figure 5A). On Day 3, no difference was observed. Thus, PAR4 activation promoted IAV-induced inflammation of the lungs at later time points postinfection. Similarly, staining of lung sections on Day 6 revealed marked cellular infiltrates of leukocytes (H&E) and neutrophils (Ly6G) in the lungs of PAR4-AP–treated mice compared with control animals (Figure 5B). Similar numbers of IAV-infected cells were detected by immunohistochemistry

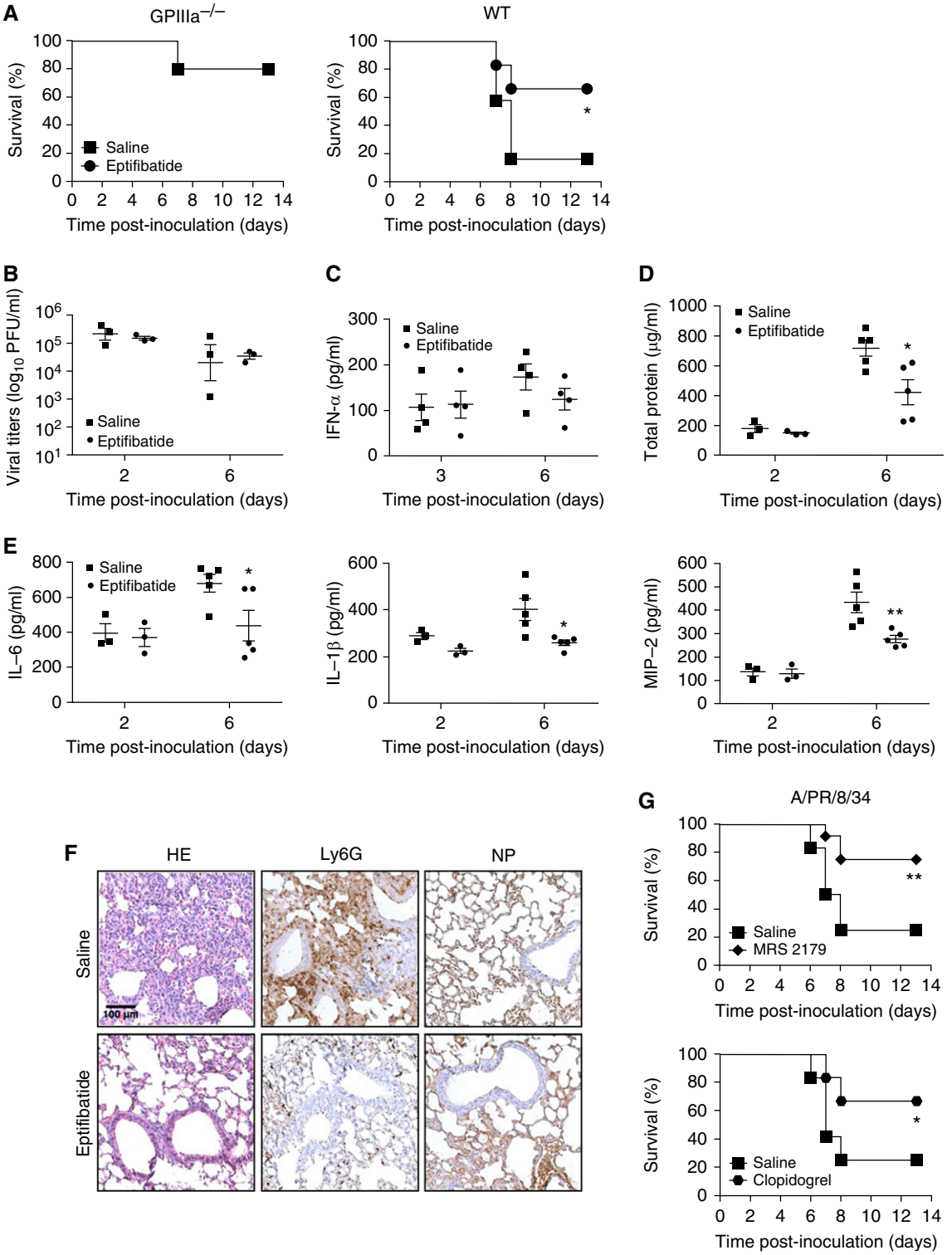

Figure 8. Eptifibatide treatment prevents severe inflammation during influenza virus infections. (*A*) Survival of glycoprotein (GP) IIIa$^{-/-}$ (n = 5 mice per group) and wild-type (WT) mice (n = 12 mice per group) after infection with influenza A virus A/PR/8/34 (300 pfu per mouse) and treatment or no treatment with eptifibatide. *$P < 0.05$ for eptifibatide versus saline. (*B*) Lung virus titers after infection of mice with the A/NL/602/09 virus (30,000 pfu per mouse; 50% lethal dose [LD_{50}]) treated with eptifibatide or vehicle. Data represent the means ± SEM from three individual animals per group. (*C*) IFN-α was measured by ELISA in the bronchoalveolar lavage (BAL) of infected mice (A/PR/8/34; 250 pfu per mice) after treatment with eptifibatide or vehicle. The results represent the means ± SEM of four mice per group. (*D* and *E*) Total proteins and levels of cytokines were determined by ELISA in the BAL of infected mice (30,000 pfu per mouse; A/NL/602/09; LD_{50}) after treatment with eptifibatide or vehicle. The results represent the means ± SEM of

using an anti-NP antibody. No staining was observed in the lungs of uninfected control mice.

PAR4 Antagonism Protects against Influenza Virus Pathogenicity

When mice were infected with IAV A/PR/8/34 (LD_{50}), treatment with pepducin p4pal-10 protected them from death (Figure 6A). Substantial protection was also observed against infection with an H3N2 virus, A/HK/1/68. The protection conferred by PAR4 antagonism correlated with the degree of inhibition of platelet activation. In the BAL of pepducin p4pal-10–treated mice, decreased TXB_2, a specific marker of platelet activation, was observed (Figure 6B). In contrast, no difference in the mean lung virus titers was detected on Day 3 or 6 after inoculation with IAV A/PR/8/34 (Figure 6C). However, treatment with pepducin p4pal-10 significantly reduced the recruitment of leukocytes (Figure 6D), including neutrophils, in BAL on Day 6. Total proteins (Figure 6E) and IL-6, IL-1β, and MIP-2 (Figure 6F) were also decreased. Consistent with those results, histopathology revealed that treatment with pepducin p4pal-10 reduced infiltration of inflammatory cells (H&E), including neutrophils (Ly6G), in the lungs of infected mice (Figure 6G), whereas similar numbers of IAV-infected cells (NP) were detected by immunohistochemistry.

The Antiplatelet Drug Eptifibatide Protects Mice from Lethal Influenza Infection

Mice were inoculated with IAV A/PR/8/34 (LD_{50}) and were treated or not with 500 μg/kg of eptifibatide every 3 days. This dosage is comparable with the lowest doses used clinically in humans (20–22). Eptifibatide treatment had a dramatic effect on lung infiltration by platelets: platelet aggregation was totally prevented, and only isolated platelets were observed (Figure 7A). Furthermore, this effect was accompanied by decreases in TXB_2 and sP-selectin in the fluid of infected mice compared with control animals (Figure 7B), showing that inhibition of platelet aggregation also limited the extent of platelet activation. More importantly, treatment with eptifibatide improved the outcome of infection with A/PR/8/34 virus and prevented mortality of the mice (Figure 7C). Protection was also observed with other influenza strains. No effect of eptifibatide was observed in $GPIIIa^{-/-}$ mice (Figure 8A), showing the specificity of the drug.

The protective effect of eptifibatide was independent of virus replication in lungs (Figure 8B) and IFN-α release in the BAL (Figure 8C). In contrast, it was correlated with decreased total proteins and levels of certain cytokines in the BAL of eptifibatide-treated mice (Figures 8D and 8E). Immunohistochemistry confirmed that treatment by eptifibatide prevented IAV-induced lung alveolar damage (H&E) and neutrophil infiltration (Ly6G) but not viral replication (NP) on Day 6 postinfection (Figure 8F). This effect was not observed on Day 2 (data not shown). Treatment of infected mice with MRS 2179 and clopidogrel, which inhibits the adenosine diphosphate receptors P2Y1 and P2Y12, improved the outcome of IAV infection (Figure 8G).

Eptifibatide Treatment Protects Mice from Lung Injury Induced by Influenza

Histopathologic analyses of lung tissues were performed to evaluate the extent of hemorrhage after eptifibatide treatment. Mice were infected with A/PR/8/34 virus and treated with eptifibatide or vehicle, and lungs were then harvested 6 days postinoculation for histopathology. In the infected group, lungs presented signs of congestion with infiltration of neutrophils and monocytes, interstitial and alveolar hemorrhages, and thrombosis (Figure 9A). Fibrin and erythrocyte-rich thrombi were observed in small vessels. Figure 9B summarizes the blinded semiquantitative scoring of the different parameters. Eptifibatide markedly reduced the severity of pulmonary injury induced by influenza virus infections, and a marked reduction in neutrophil infiltration was observed (Figures 9A and 9B). More importantly, almost no hemorrhage was detected in the lungs of infected mice treated with eptifibatide.

Discussion

The present study shows that platelets play an active role in fueling the dysregulation of inflammation and promoting pathogenesis of influenza virus infections. Histologic analysis of lungs provided evidence that platelets massively infiltrate the lungs of infected mice. Additionally, infiltrated platelets stained positive for viral HA, based on immunofluorescence staining of BAL and immunogold labeling of ultrathin cryosections of lungs. The technical limitation of the staining did not allow us to determine whether platelets engulfed the entire virions, only IAV fragments or antigens. However, because platelets incorporate influenza viruses *in vitro* (23), our results suggest that platelets recruited to the lungs most likely take up IAV particles *in vivo* as well. This could consist of a passive passage of particles through the open canalicular system, the tortuous invaginations of platelet surface membranes tunneling through the cytoplasm, in a manner similar to bacterial ingestion (24). Alternatively, uptake of IAVs may be compared with phagocytosis by macrophages and neutrophils, as previously observed for human immunodeficiency viruses (25).

Ultrastructural analysis showed that features of platelets in the lungs of infected mice are those of aggregates of activated platelets: platelets were tightly stacked without interplatelet spaces, and some platelets were devoid of granules, suggesting that they had degranulated. Consistent with those observations, markers of platelet activation were detected in the BAL and plasma of infected mice. Thus, on lethal IAV infection, platelets are activated in the lung and in the peripheral circulation. Our observations are consistent with the

Figure 8. (Continued). three to five mice per group. $^{*}P < 0.05$, $^{**}P < 0.01$ for eptifibatide versus saline. (*F*) Histopathologic analysis of lungs from mice infected with A/NL/602/09 virus (30,000 pfu per mouse; LD_{50}) after treatment with eptifibatide or vehicle, on Day 6 postinfection. Lung sections were stained with hematoxylin and eosin (HE). Immunohistochemistry using antibodies against Ly6G and viral nucleoprotein (NP) was used to detect neutrophils and virus-infected cells. Data are representative of three mice per group. (*G*) Survival of mice treated with MRS 2179, clopidogrel, or vehicle after infection with influenza A virus A/PR/8/34 (250 pfu per mouse; n = 12 mice per group). $^{**}P < 0.01$ for MRS 2179 versus saline; $^{*}P < 0.05$ for clopidogrel versus saline. MIP = macrophage inflammatory protein.

A

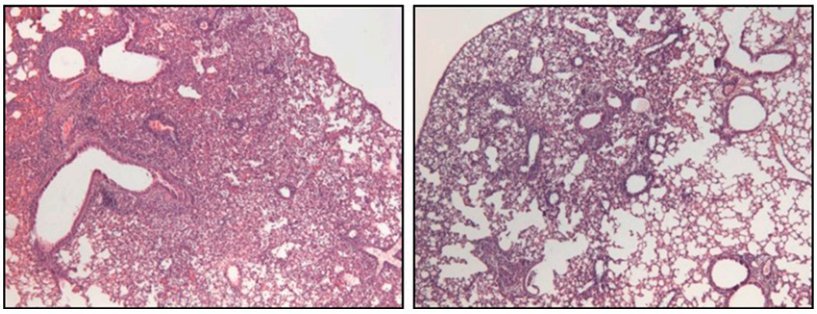

B

		Saline			Eptifibatide		
	Mouse	1	2	3	1	2	3
Neutrophil infiltration	Alveoli	++	+	+	+	+	+
	Bronchiole	++	+	+	+	+	+
	Bronchus	++	+	+	+	+	+
	Interalveolar septa	++	++	++	+	+	+
	Peribronchiolar parenchyma	++	++	++	+	+	+
	Big vessels	–	–	–	–	–	–
	Serosa	–	–	–	–	–	–
Mononuclear cell infiltration	Alveoli	+++	+++	+++	++	++	++
	Bronchiole	+++	+++	+++	++	++	++
	Bronchus	+++	+++	+++	++	++	++
	Interalveolar septa	+++	+++	+++	++	++	++
	Peribronchiolar parenchyma	+++	+++	+++	+++	+++	+++
	Big vessels	–	–	–	–	–	–
	Serosa	–	–	–	–	–	–
Vascular congestion	Alveoli	+++	++	++	–	–	+
	Bronchiole	+++	++	++	–	–	++
	Bronchus	+++	++	++	–	–	++
	Interalveolar septa	+++	++	++	–	–	++
	Peribronchiolar parenchyma	+++	++	++	–	–	++
	Big vessels	+++	++	++	+	+	++
	Serosa	+++	++	++	–	–	–
Hemorrhage	Alveoli	++	++	+	–	–	+
	Bronchiole	+	+	+	–	–	–
	Bronchus	–	–	–	–	–	–
	Interalveolar septa	–	–	–	–	–	–
	Peribronchiolar parenchyma	–	–	–	–	–	–
	Big vessels	–	–	–	–	–	–
	Serosa	–	–	–	–	–	–
Fibrin deposit	Alveoli	+++	++	++	–	–	–
	Bronchiole	–	–	–	–	–	–
	Bronchus	–	–	–	–	–	–
	Interalveolar septa	–	–	–	–	–	–
	Peribronchiolar parenchyma	–	–	–	–	–	–
	Big vessels	–	–	–	–	–	–
	Serosa	–	–	–	–	–	–
Epithelial cell apoptosis	Alveoli	++	++	++	–	–	+
	Bronchiole	++	++	++	–	–	–
	Bronchus	++	++	++	+	+	+
	Interalveolar septa	–	–	–	–	–	–
	Peribronchiolar parenchyma	–	–	–	–	–	–
	Big vessels	–	–	–	–	–	–
	Serosa	–	–	–	–	–	–

Figure 9. Histopathologic analysis of lungs from infected mice after treatment with eptifibatide. (*A*) Histopathologic analysis of lungs obtained from mice inoculated with A/PR/8/34 virus (250 pfu per mouse) and treated or not with eptifibatide. In the infected (INF) group, note the extended areas with interstitial and peribronchial inflammation and interstitial and alveolar hemorrhage. In the INF group treated with eptifibatide, note the limited areas with slight peribronchial inflammation but no major hemorrhage. (*B*) Blinded semiquantitative scoring of inflammatory infiltration, vascular congestion, hemorrhage, fibrin deposits, and epithelial cell apoptosis in the lungs of infected mice treated or not with eptifibatide. All lung fields were examined (50×) for each sample. The scoring was performed as follows: – = no lesion, + = mild, ++ = moderate, +++ = severe.

recent findings that influenza virus activates platelets through FcγRIIA signaling or thrombin generation (26). Also, thrombin triggers the release of serotonin and TXA_2 from platelets, promotes P-selectin translocation to the platelet plasma membrane, and activates the GPIIb/IIIa complex (27).

Platelets contribute to the host defense against bacterial infectious agents by limiting vascular lesions and inducing injury repair (28, 29). However, unbalanced platelet activation may have pathologic consequences. In the IAV infection model used in this study, platelet activation and aggregation proved to be deleterious. PAR4 and GPIIIa are both key molecules in platelet function. PAR4 is strictly required for platelet activation in mice, whereas GPIIIa is required for platelet aggregation. First, mice deficient in GPIIIa were protected from lung injury and death. Furthermore, stimulation of PAR4 increased lung inflammation and the severity of IAV infection. In contrast, PAR4 antagonists protected mice from death. Our results indicate that PAR4 acts through platelet activation because the effect of PAR4-AP was abrogated when infected mice were treated with the platelet-specific inhibitor eptifibatide (30), or when mice were deficient in platelet GPIIIa protein. Altogether, the data indicate that platelets regulate IAV pathogenesis.

Interestingly, the observation by others that influenza virus activates platelets through thrombin generation (26) suggests that thrombin may also act in a deleterious manner against IAV infection. Thrombin mediates signal transduction mainly by activating PAR4 and PAR1 (31, 32). Because mouse platelets do not express PAR1, thrombin-mediated platelet activation most likely occurs through PAR4 activation, but thrombin activation of PAR1 may also be involved in the pathogenesis of IAV infection. Indeed, we recently found that PAR1 signaling contributes to IAV pathogenicity in mice (33). In this context, PAR1 cooperates with plasminogen, which controls pathogenesis, via fibrinolysis (34). Thus, investigations into the role of hemostasis dysregulation may help better understand IAV pathogenesis (35–37).

In several models of injury, uncontrolled platelet activation drives deleterious inflammation (38). Activated platelets release an arsenal of potent proinflammatory molecules (39), which exacerbate neutrophil rolling, adhesion, and recruitment (40–42). In addition, the physical interaction between platelets and neutrophils further contributes to neutrophil retention and activation (42). Because dysregulation of inflammation is a hallmark of severe influenza virus infections, it is likely that platelets have a proinflammatory effect with a key role in IAV pathogenesis. In our study, electron microscopy demonstrated the presence of neutrophil-platelet complexes on IAV infection. The antiplatelet molecule eptifibatide inhibited neutrophil recruitment into inflamed lungs (Figure 9). Thus, platelet interaction with neutrophils is likely to play a role during severe inflammation induced by influenza.

Interestingly, the exacerbation of cytokine production induced by platelet activation was only observed at later time points after infection. On infection, the virus is recognized as foreign by highly conserved receptors known as pattern recognition receptors. Activation of these receptors results in the secretion of cytokines and chemokines, which corresponds to the early inflammatory response against IAV infection (35). Thus, the amplification and intensity of inflammation depends on the replicative capacity of the virus. When the response is tightly controlled, a resolution phase of inflammation is engaged at later time points postinfection, and this partly determines the duration of inflammation. Resolution of inflammation is largely influenced by the vascular endothelium (43). On injury of the latter, platelets are activated. Our data show coordinated platelet activation/aggregation and inflammatory responses at late time points postinfection, indicating that platelets may affect the recovery phase after infection and wound healing. In this scenario, extravasation of large numbers of platelets and leukocytes would be the basis of the defect in the resolution phase of the inflammation. Most likely, this further promotes hemostasis dysregulation, such as fibrinolysis (18, 35) or PAR1 activation (33, 44), fueling the vicious circle of inflammation (34, 35).

Recurrent outbreaks of IAV that cause severe infections in humans have raised serious concerns about therapeutic strategies available for these pathogens. Current treatments that target viral proteins have a number of disadvantages, including the rapid development of resistant virus variants as a result of selective pressure (45, 46). Because targeting the host rather than the virus would not easily lead to resistance, drugs regulating inflammation are appealing as potential new therapeutics for IAV symptoms (13, 33, 34, 47). Here, we found that available antiplatelet drugs efficiently protected mice from IAV pathogenesis induced by several influenza strains. These results are consistent with other studies showing that aspirin, known to inhibit platelet activation, blocks IAV propagation via nuclear factor-κB inhibition (48). Altogether, these results suggest that antiplatelet drugs might be explored as new antiinflammatory treatments against severe influenza. ■

Author disclosures are available with the text of this article at www.atsjournals.org.

Acknowledgment: Authors are grateful to Dr. P. Clézardin (Inserm UMR S1033, France) and Dr. C. Dumontet (Cancer Center of Lyon, France) for help with the immunohistochemistry and immunofluorescence.

References

1. Kuiken T, Riteau B, Fouchier RA, Rimmelzwaan GF. Pathogenesis of influenza virus infections: the good, the bad and the ugly. *Curr Opin Virol* 2012;2:276–286.
2. Fukuyama S, Kawaoka Y. The pathogenesis of influenza virus infections: the contributions of virus and host factors. *Curr Opin Immunol* 2011;23:481–486.
3. Foucault ML, Moules V, Rosa-Calatrava M, Riteau B. Role for proteases and HLA-G in the pathogenicity of influenza A viruses. *J Clin Virol* 2011;51:155–159.
4. Cheung CY, Poon LL, Lau AS, Luk W, Lau YL, Shortridge KF, Gordon S, Guan Y, Peiris JS. Induction of proinflammatory cytokines in human macrophages by influenza A (H5N1) viruses: a mechanism for the unusual severity of human disease? *Lancet* 2002;360: 1831–1837.
5. de Jong MD, Simmons CP, Thanh TT, Hien VM, Smith GJ, Chau TN, Hoang DM, Chau NV, Khanh TH, Dong VC, *et al*. Fatal outcome of human influenza A (H5N1) is associated with high viral load and hypercytokinemia. *Nat Med* 2006;12: 1203–1207.

6. Kobasa D, Jones SM, Shinya K, Kash JC, Copps J, Ebihara H, Hatta Y, Kim JH, Halfmann P, Hatta M, *et al*. Aberrant innate immune response in lethal infection of macaques with the 1918 influenza virus. *Nature* 2007;445:319–323.
7. Teijaro JR, Walsh KB, Cahalan S, Fremgen DM, Roberts E, Scott F, Martinborough E, Peach R, Oldstone MB, Rosen H. Endothelial cells are central orchestrators of cytokine amplification during influenza virus infection. *Cell* 2011;146:980–991.
8. Rumbaut RE, Thiagarajan P. Platelet-vessel wall interactions in hemostasis and thrombosis. San Rafael, CA: Morgan & Claypool Life Sciences; 2010.
9. Duerschmied D, Suidan GL, Demers M, Herr N, Carbo C, Brill A, Cifuni SM, Mauler M, Cicko S, Bader M, *et al*. Platelet serotonin promotes the recruitment of neutrophils to sites of acute inflammation in mice. *Blood* 2013;121:1008–1015.
10. Cohen J. The immunopathogenesis of sepsis. *Nature* 2002;420:885–891.
11. Degen JL, Bugge TH, Goguen JD. Fibrin and fibrinolysis in infection and host defense. *J Thromb Haemost* 2007;5:24–31.
12. Riteau B, Moreau P, Menier C, Khalil-Daher I, Khosrotehrani K, Bras-Goncalves R, Paul P, Dausset J, Rouas-Freiss N, Carosella ED. Characterization of HLA-G1, -G2, -G3, and -G4 isoforms transfected in a human melanoma cell line. *Transplant Proc* 2001;33:2360–2364.
13. Khoufache K, LeBouder F, Morello E, Laurent F, Riffault S, Andrade-Gordon P, Boullier S, Rousset P, Vergnolle N, Riteau B. Protective role for protease-activated receptor-2 against influenza virus pathogenesis via an IFN-gamma-dependent pathway. *J Immunol* 2009;182:7795–7802.
14. Riteau B, de Vaureix C, Lefèvre F. Trypsin increases pseudorabies virus production through activation of the ERK signalling pathway. *J Gen Virol* 2006;87:1109–1112.
15. Riteau B, Faure F, Menier C, Viel S, Carosella ED, Amigorena S, Rouas-Freiss N. Exosomes bearing HLA-G are released by melanoma cells. *Hum Immunol* 2003;64:1064–1072.
16. LeBouder F, Morello E, Rimmelzwaan GF, Bosse F, Péchoux C, Delmas B, Riteau B. Annexin II incorporated into influenza virus particles supports virus replication by converting plasminogen into plasmin. *J Virol* 2008;82:6820–6828.
17. Berri F, Haffar G, Lê VB, Sadewasser A, Paki K, Lina B, Wolff T, Riteau B. Annexin V incorporated into influenza virus particles inhibits gamma interferon signaling and promotes viral replication. *J Virol* 2014;88:11215–11228.
18. LeBouder F, Lina B, Rimmelzwaan GF, Riteau B. Plasminogen promotes influenza A virus replication through an annexin 2-dependent pathway in the absence of neuraminidase. *J Gen Virol* 2010;91:2753–2761.
19. LeBouder F, Khoufache K, Menier C, Mandouri Y, Keffous M, Lejal N, Krawice-Radanne I, Carosella ED, Rouas-Freiss N, Riteau B. Immunosuppressive HLA-G molecule is upregulated in alveolar epithelial cells after influenza A virus infection. *Hum Immunol* 2009; 70:1016–1019.
20. Hassan W, Al-Sergani H, Al Buraiki J, Dunn B, Al Turki F, Akhras N, Elshaer F, Nawaz M, Kharabsheh S, ElKum N. Immediate and intermediate results of intracoronary stand-alone bolus administration of eptifibatide during coronary intervention (ICE) study. *Am Heart J* 2007;154:345–351.
21. Gilchrist IC, O'Shea JC, Kosoglou T, Jennings LK, Lorenz TJ, Kitt MM, Kleiman NS, Talley D, Aguirre F, Davidson C, *et al*. Pharmacodynamics and pharmacokinetics of higher-dose, double-bolus eptifibatide in percutaneous coronary intervention. *Circulation* 2001;104:406–411.
22. Tcheng JE, Talley JD, O'Shea JC, Gilchrist IC, Kleiman NS, Grines CL, Davidson CJ, Lincoff AM, Califf RM, Jennings LK, *et al*. Clinical pharmacology of higher dose eptifibatide in percutaneous coronary intervention (the PRIDE study). *Am J Cardiol* 2001;88:1097–1102.
23. Danon D, Jerushalmy Z, De Vries A. Incorporation of influenza virus in human blood platelets in vitro. Electron microscopical observation. *Virology* 1959;9:719–722.
24. White JG. Platelets are covercytes, not phagocytes: uptake of bacteria involves channels of the open canalicular system. *Platelets* 2005;16: 121–131.
25. Youssefian T, Drouin A, Massé JM, Guichard J, Cramer EM. Host defense role of platelets: engulfment of HIV and *Staphylococcus aureus* occurs in a specific subcellular compartment and is enhanced by platelet activation. *Blood* 2002;99:4021–4029.
26. Boilard E, Paré G, Rousseau M, Cloutier N, Dubuc I, Lévesque T, Borgeat P, Flamand L. Influenza virus H1N1 activates platelets through FcγRIIA signaling and thrombin generation. *Blood* 2014;123: 2854–2863.
27. Polley MJ, Leung LL, Clark FY, Nachman RL. Thrombin-induced platelet membrane glycoprotein IIb and IIIa complex formation. An electron microscope study. *J Exp Med* 1981;154:1058–1068.
28. Petäjä J. Inflammation and coagulation. An overview. *Thromb Res* 2011;127:S34–S37.
29. Engelmann B, Massberg S. Thrombosis as an intravascular effector of innate immunity. *Nat Rev Immunol* 2013;13:34–45.
30. Tardiff BE, Jennings LK, Harrington RA, Gretler D, Potthoff RF, Vorchheimer DA, Eisenberg PR, Lincoff AM, Labinaz M, Joseph DM, *et al*.; PERIGEE Investigators. Pharmacodynamics and pharmacokinetics of eptifibatide in patients with acute coronary syndromes: prospective analysis from PURSUIT. *Circulation* 2001; 104:399–405.
31. Kahn ML, Nakanishi-Matsui M, Shapiro MJ, Ishihara H, Coughlin SR. Protease-activated receptors 1 and 4 mediate activation of human platelets by thrombin. *J Clin Invest* 1999;103:879–887.
32. Kataoka H, Hamilton JR, McKemy DD, Camerer E, Zheng YW, Cheng A, Griffin C, Coughlin SR. Protease-activated receptors 1 and 4 mediate thrombin signaling in endothelial cells. *Blood* 2003;102: 3224–3231.
33. Khoufache K, Berri F, Nacken W, Vogel AB, Delenne M, Camerer E, Coughlin SR, Carmeliet P, Lina B, Rimmelzwaan GF, *et al*. PAR1 contributes to influenza A virus pathogenicity in mice. *J Clin Invest* 2013;123:206–214.
34. Berri F, Rimmelzwaan GF, Hanss M, Albina E, Foucault-Grunenwald ML, Lê VB, Vogelzang-van Trierum SE, Gil P, Camerer E, Martinez D, *et al*. Plasminogen controls inflammation and pathogenesis of influenza virus infections via fibrinolysis. *PLoS Pathog* 2013;9: e1003229.
35. Berri F, Lê VB, Jandrot-Perrus M, Lina B, Riteau B. Switch from protective to adverse inflammation during influenza: viral determinants and hemostasis are caught as culprits. *Cell Mol Life Sci* 2014;71:885–898.
36. Antoniak S, Mackman N. Multiple roles of the coagulation protease cascade during virus infection. *Blood* 2014;123:2605–2613.
37. Pryzdial EL, Sutherland MR, Ruf W. The procoagulant envelope virus surface: contribution to enhanced infection. *Thromb Res* 2014;133: S15–S17.
38. Henn V, Slupsky JR, Gräfe M, Anagnostopoulos I, Förster R, Müller-Berghaus G, Kroczek RA. CD40 ligand on activated platelets triggers an inflammatory reaction of endothelial cells. *Nature* 1998;391: 591–594.
39. von Hundelshausen P, Weber KS, Huo Y, Proudfoot AE, Nelson PJ, Ley K, Weber C. RANTES deposition by platelets triggers monocyte arrest on inflamed and atherosclerotic endothelium. *Circulation* 2001;103:1772–1777.
40. Diacovo TG, Roth SJ, Buccola JM, Bainton DF, Springer TA. Neutrophil rolling, arrest, and transmigration across activated, surface-adherent platelets via sequential action of P-selectin and the beta 2-integrin CD11b/CD18. *Blood* 1996;88:146–157.
41. Mayadas TN, Johnson RC, Rayburn H, Hynes RO, Wagner DD. Leukocyte rolling and extravasation are severely compromised in P selectin-deficient mice. *Cell* 1993;74:541–554.
42. Zarbock A, Polanowska-Grabowska RK, Ley K. Platelet-neutrophil-interactions: linking hemostasis and inflammation. *Blood Rev* 2007; 21:99–111.
43. Kadl A, Leitinger N. The role of endothelial cells in the resolution of acute inflammation. *Antioxid Redox Signal* 2005;7:1744–1754.
44. Aerts L HM, Rhéaume C, Lavigne S, Couture C, Kim W, Susan-Resiga D, Prat A, Seidah NG, Vergnolle N, Riteau B, *et al*. Modulation of protease activated receptor 1 influences human metapneumovirus disease severity in a mouse model. *PLoS One* 2013;28;8:e72529.

45. Song MS, Hee Baek Y, Kim EH, Park SJ, Kim S, Lim GJ, Kwon HI, Pascua PN, Decano AG, Lee BJ, *et al*. Increased virulence of neuraminidase inhibitor-resistant pandemic H1N1 virus in mice: potential emergence of drug-resistant and virulent variants. *Virulence* 2013;4:489–493.
46. Butler J, Hooper KA, Petrie S, Lee R, Maurer-Stroh S, Reh L, Guarnaccia T, Baas C, Xue L, Vitesnik S, *et al*. Estimating the fitness advantage conferred by permissive neuraminidase mutations in recent oseltamivir-resistant A(H1N1)pdm09 influenza viruses. *PLoS Pathog* 2014;10:e1004065.
47. Walsh KB, Teijaro JR, Wilker PR, Jatzek A, Fremgen DM, Das SC, Watanabe T, Hatta M, Shinya K, Suresh M, *et al*. Suppression of cytokine storm with a sphingosine analog provides protection against pathogenic influenza virus. *Proc Natl Acad Sci USA* 2011; 108:12018–12023.
48. Mazur I, Wurzer WJ, Ehrhardt C, Pleschka S, Puthavathana P, Silberzahn T, Wolff T, Planz O, Ludwig S. Acetylsalicylic acid (ASA) blocks influenza virus propagation via its NF-kappaB-inhibiting activity. *Cell Microbiol* 2007;9: 1683–1694.